Title	Extended wavelength anisotropy resolved multidimensional emission spectroscopy (ARMES) measurements: better filters, validation standards, and Rayleigh scatter removal methods
Author(s)	Casamayou-Boucau, Yannick; Ryder, Alan G.
Publication Date	2017-08-17
Publication Information	Casamayou-Boucau, Yannick, & Ryder, Alan G. (2017). Extended wavelength anisotropy resolved multidimensional emission spectroscopy (ARMES) measurements: better filters, validation standards, and Rayleigh scatter removal methods. Methods and Applications in Fluorescence, 5(037001). doi: 10.1088/2050-6120/aa7763
Publisher	IOP Publishing
Link to publisher's version	https://doi.org/10.1088/2050-6120/aa7763
Item record	http://hdl.handle.net/10379/14646
DOI	http://dx.doi.org/10.1088/2050-6120/aa7763

Author version: Revised but not proof corrected. The final published version can be accessed here:
Citation: Y. Casamayou-Boucau and A.G. Ryder. *Methods and Applications in Fluorescence*, 5, 037001, (**2017**). DOI: 10.1088/2050-6120/aa7763

Extended wavelength Anisotropy Resolved Multidimensional Emission Spectroscopy (ARMES) measurements: *better filters, validation standards, and Rayleigh scatter removal methods.*

Yannick Casamayou-Boucau and Alan G. Ryder.*
Nanoscale BioPhotonics Laboratory, School of Chemistry, National University of Ireland, Galway, Galway, Ireland.

* Corresponding author: **Email:** alan.ryder@nuigalway.ie, **Phone:** +353-91-492943.
Postal address: Nanoscale Biophotonics Laboratory, School of Chemistry, National University of Ireland, Galway, University Road, Galway, H91TK33, Ireland.

Running Title: Multidimensional fluorescence anisotropy measurements in the UV.

Abstract:

Anisotropy resolved multidimensional emission spectroscopy (ARMES) provides valuable insights into multi-fluorophore proteins [1]. Fluorescence anisotropy adds to the multidimensional fluorescence (MDF) dataset, information about the physical size of the fluorophores and/or the rigidity of the surrounding micro-environment. The first ARMES studies used standard thin film polarizers (TFP) that had negligible transmission between 250 and 290 nm, preventing accurate measurement of intrinsic protein fluorescence from Tyrosine and Tryptophan. Replacing TFP with pairs of broadband Wire Grid Polarizers (WGP) enabled standard fluorescence spectrometers to accurately measure anisotropies between 250 and 300 nm, which was validated with solutions of perylene in the UV and Erythrosin B and Phloxine B in the visible. In all cases, anisotropies were accurate to better than ±1% when compared to literature measurements made with Glan Thompson or TFP polarizers. Better dWGP UV transmittance and the use of excitation emission matrix measurements for ARMES required complete Rayleigh scatter elimination. This was achieved by chemometric modelling rather than classical interpolation, which enabled the acquisition of pure anisotropy patterns over wider spectral ranges. In combination, these three improvements permit the accurate implementation of ARMES for studying intrinsic protein fluorescence.

Keywords: Fluorescence, Anisotropy, Multidimensional, Standards, Polarizers, Rayleigh Scatter, Chemometrics.

1. Introduction.

1.1 Intrinsic Protein Fluorescence: Protein analysis by measurement of intrinsic fluorescence is very attractive because it minimizes sample modifications which can adversely impact the structure, stability, and behavior of the native state [2-6]. To fully explore fluorescence behavior it is necessary to use multidimensional fluorescence spectroscopy (MDF) techniques like excitation-emission matrix (EEM) [7] and Total Synchronous Fluorescence Scan (TSFS) [8], which are spectral fingerprints of the multiple fluorophores present in a protein or a complex sample [9, 10]. One problem with multi-fluorophore systems is that extensive spectral band overlap can make spectral interpretation difficult. Multivariate curve resolution (MCR) [11-14], and parallel factor analysis (PARAFAC) [15-17] can be used to identify the spectral contributions of individual constituents. However, even with chemometric

analysis, fluorophore emission can remain unresolved, so one needs to measure other properties (*e.g.* lifetime, anisotropy) to enable fluorophore resolution.

1.2 Anisotropy Resolved Multi-dimensional Emission Spectroscopy (ARMES): Combining anisotropy with MDF [18] enabled the differentiation and quantification of fluorophores with similar emission properties in complex mixtures, based on their rotational speed and hydrodynamic volume, and thus molecular size, or for macromolecules the mobility/flexibility of constituent fluorophores. In the first ARMES studies using TSFS measurements with a standard fluorescence spectrometer fitted with TFP [1, 18, 19], we observed that multi-fluorophore proteins (BSA/HSA) generated complex *aniso*-TSFS (excitation wavelength (λ_{ex}), wavelength offset ($\Delta\lambda$), anisotropy (r)) patterns diagnostic of protein structure and stability. However, because of negligible TFP transmission below ~290 nm, the full emission signal could not be collected. TFP also caused excitation maxima of recovered components to be red-shifted and reshaped, compared to non-polarized spectra [1, 19]. While this distortion compensated for the lack of trilinearity in TSFS data, it also distorted the recovered excitation profiles which often appeared to have dual bands, an artefact caused by the TSFS data structure. To solve these problems is the focus of this note and required the use of polarizers with better UV transmittance, the use of a UV anisotropy standard, and implementation of accurate Rayleigh scatter correction:

1.3 Polarizers: To use ARMES for intrinsic protein fluorescence, it was critical to be able to collect efficiently polarized fluorescence data in the 250–400 nm region where the main amino-acids responsible for protein fluorescence absorb and emit (SI, Fig. S-2). The compact sample compartments of most standard fluorimeters (a Cary Eclipse here) meant there was insufficient space for installing more efficient cube type designs such as Glan-Thompson polarizers (GTP) [20]. The only practical solution was to use pairs of broadband Wire Grid Polarizers (WGP) which were similar in size to TFP.

1.4 UV Standard: An effective UV anisotropy standard was needed for validating dual WGP (dWGP) efficacy, using conventional anisotropy measurements. However, standards are rare in this wavelength range (see supplemental information, SI). Perylene [21-23] was selected because it has two UV excitation bands, it is stable and can be measured at room temperature (20–25°C) in glycerol (safe solvent). These bands correspond to two electronic states oriented along orthogonal molecular symmetry axes, thus generating different anisotropies [21, 24], with a short wavelength band ($S_0 \rightarrow S_2$) oriented along the short symmetry axis, and the longer

excitation wavelength band ($S_0 \rightarrow S_1$) oriented along the long symmetry axis [2]. Emission is always from S_1 at ~440 nm, yielding two band pairs: $\lambda_{ex/em}$ = 254 nm/440 nm, and ~ 434/440 nm. According to Kasha's rule, the emission dipole is oriented along the same axis as the $S_0 \rightarrow S_1$ absorption dipole, producing a theoretical angle α, of 0° and 90° respectively for $S_0 \rightarrow S_1$ and $S_0 \rightarrow S_2$ transitions, yielding fundamental anisotropies of 0.4 (λ_{ex} > 300 nm), and –0.2 for (λ_{ex} < 300 nm) [25]. Cryogenic measurements of the $S_0 \rightarrow S_1$ band in various solvents were reported by Johansson [24] and Pantke [26]. For ambient temperature measurements, the literature is sparse and the most comprehensive report was from Barkley [21]. Validation was undertaken in the visible spectral region using Erythrosin B and Phloxine B.

1.5 Scatter Correction: One consequence of using dWGP with better UV transmittance was the loss of the cut-off point at ~290 nm [1, 19], which resulted in the loss of the trilinear behavior previously observed for TSFS measurements. Concretely this meant that the resolution of meaningful components by MCR for dWGP-TSFS data was impossible, and natural trilinear EEM measurements [27] were required. However when EEM are contaminated by strongly polarized Rayleigh scatter it generates erroneous anisotropy data [2], and disrupts the implementation of curve resolution methods [28, 29]. Instead of using classical interpolation based correction, we found out that modelling of shifted scatter by PCA or PARAFAC [30] was more efficient and generated EEM data that were completely Rayleigh free, enabling accurate anisotropy measurements over a much wider emission range.

2. Experimental Section.

2.1 Materials: Glycerol (spectrophotometric grade, Acros Organics), HEPES buffer (Sigma), perylene (analytical standard), Erythrosin B, and Phloxine B (from Sigma-Aldrich) were used as received without further purification. Stock solutions of 1 μM perylene in glycerol, and Erythrosin B (6 μM), and Phloxine B (0.6 μM) in 50 mM HEPES buffer (pH = 7.2) were stored at −20°C, and defrosted overnight at 2-8°C prior to measurement. These concentrations were chosen to limit reabsorption effects and generate similar fluorescence intensities.

2.2 Optical Components: The TFP were standard Agilent components mounted either in a manual polarizer accessory (#00-100761-00) or an automated polarizer accessory (#8510187100). Ultra-broadband WGP (Thorlabs, 25 mm diameter, #WP25M-UB) were mounted in pairs in indexing rotation mounts (Thorlabs). To assemble these mounts, two filters were carefully aligned, fixed together and tightly screwed to ensure that no movement could occur during mount rotation. These were then fixed in a homebuilt holder, similar to the

Agilent manual polarizer accessory (SI, Fig. S-1). The alignment of filter pairs was then verified by checking that no light was passing for crossed polarizer positions (HV and VH).

2.3 Instrumentation and data collection: Filter transmittance spectra were recorded on a Cary 60 UV-Visible spectrometer at normal incidence. Each of the filters has a vertical (V) and horizontal (H) setting, and was used else in excitation (Ex) or emission (Em) pathlengths. Fluorescence data were measured in triplicate at temperatures varying from 10 to 25°C from solutions in 0.4×1 cm pathlength quartz cuvettes (Lightpath Optical, UK) using an Eclipse fluorimeter (Agilent) fitted with a modified manual polarizer accessory and a thermostatted multi-cell holder. Samples were thermally equilibrated for several minutes prior to measurements. Perylene EEM data were collected over λ_{ex} = 230–470 nm and λ_{em} of 420-530 nm ranges (2 nm step increments) with 5 and 10 nm excitation/emission slit widths. TSFS measurements were collected using λ_{ex} = 230–470 nm and $\Delta\lambda$ intervals of 20–210 nm. For Erythrosine B and Phloxine B, EEM were collected using 10 nm excitation/emission slit widths. Four different polarized spectra were collected: VV (*i.e.* vertical-vertical), VH, HV, HH, and used to calculate the anisotropy (r) at each $\lambda_{ex}/\lambda_{em}$ point using the following formula [2], where G (=I_{HV}/I_{HH}) corrected for instrument response:

Equation 1

$$\mathbf{r} = \frac{\mathbf{I_{VV} - G \times I_{VH}}}{\mathbf{I_{VV} + 2 \times G \times I_{VH}}}$$

3. Results and Discussion

3.1 Wire Grid Polarizers: Transmittance spectra of individual filters (Figure 1A/C) and paired assemblies (Figure 1B/D) were collected for four different polarization settings which showed that TFP were opaque below ~290 nm whereas WGP had very good transmission <290 nm. However, transmittance spectra of individual WGP were not identical, due to the difficulty in fabricating reproducible high frequency, nm sized metal gratings [31]. These small differences between filters are not a problem as long as polarizer sets are not switched between excitation and emission. Single WGP had poor extinction ratios, with significant light transmittance between 250 and 300 nm which is the primary region of interest (HV/VH spectra, Figure 1F). Poor WGP extinction ratios (~10:1) in this range was related to wires spacing and thickness [32], too close to wavelength of the incident light (SI, Tab. S-1).

This transmission of non-polarised light adversely affected the accuracy of anisotropy measurements and thus the solution was to use pairs of filters on both optical paths (*i.e.* dual-WGP or dWGP). Figure 1(E/F) shows the improvements in non-polarized light transmission

with an 0.04% average transmittance between 250 and 400 nm (HV/VH orientations) versus 0.8% with a single WGP filter. However, there was a significant (~30%) decrease in the overall polarized light transmittance (250-400 nm), *e.g.* 17.5→13.1% average transmittance in HH, 11.1%→7.9% for VV.

3.2 UV Anisotropy Standard: Perylene was selected because its two electronic states with absorption dipoles oriented along orthogonal symmetry axes (SI, Fig. S-3) gave two anisotropies of different sign, with one in the critical 250–300 nm region. Perylene in glycerol was first used to assess dWGP filter combination efficiency by comparison with literature and TFP measurements. Because of the high solvent viscosity and the orthogonality of the absorption dipoles, both excited states were expected to have their respective intensity maxima with orthogonal polarization settings (*i.e.* S_2 with HH and S_1 with VV), which was confirmed by the spectra collected using TFP, WGP and dWGP (Figure 3). The unsuitability of TFP for use <300 nm was shown in Figure 2, with no emission being measured which lead to random spurious anisotropy values (Figure 3A).

A major source of error in anisotropy measurements is Rayleigh scatter contamination. This appears in EEM as a 1st order peak ($\lambda_{ex} = \lambda_{em}$ [33]) and a 2nd order ($\lambda_{ex} = 2 \times \lambda_{em}$) due to the grating diffraction effect [34]. The almost pure polarized nature of Rayleigh scattered light [35], means that even a small degree of scattered light contamination will drastically affect the measured anisotropy [20]. In perylene EEM, 1st order Rayleigh scatter overlaps S_1 emission and the 2nd order peak the S_2 band, producing erroneous anisotropy values in those regions (Figure 3B/C and Figure 5, top). This limited the perylene working range to two regions ($\lambda_{ex/em}$ = 240–270/430-490 nm and $\lambda_{ex/em}$ = 370–430/450-520 nm). The efficiency/accuracy of the different polarizers were evaluated by comparing average anisotropy values obtained across these two wavelength ranges (

Table **1**), and their standard deviation (STD).

The dWGP measured anisotropies at 25°C were almost identical to those obtained by Barkley *et al.* [21] who obtained values of –0.031 and 0.197 ± 0.002 for a 2 μM glycerol solution of perylene at 25°C. Our errors of ± 0.004 (S_2) and ± 0.001 (S_1) were also similar and in general, dWGP obtained anisotropies were slightly better than those obtained for single WGP. TFP measurements were impossible for λ_{ex} <300 nm, but were better than the dWGP at longer wavelengths with r = 0.216±0.001. This was similar to Johansson's data (r ≈ 0.22) for perylene in glycerol at ≈ 300K [24]. The small differences were mostly related to different polarizer extinction ratios, as the measurements were otherwise made under identical conditions (diluted solutions (A ≤ 0.1) at 25°C). Johansson used GTP (extinction ratio of ~10^6)

[36] whereas Barkley used Polaroid or Polacoat polarizer, which have much lower (~10^3) extinction ratios [37, 38].

3.3 Perylene Temperature studies: To further validate dWGP, we undertook a temperature dependence study of perylene (1μM in 100% glycerol) at 25, 20, 15, and 10°C. Solutions were considered liquid at 20°C and 25°C, and in a rubbery state at 15°C and 10°C (see SI for more details). On cooling, VV spectral intensity increased and decreased for S_1 and S_2 states respectively (SI, Fig. S-4) because of increasing glycerol viscosity (100 fold between its melting and glass transition temperature [39, 40]). Average anisotropy values (
Table **2**) calculated across the Rayleigh scatter free wavelength range were almost identical to equivalent literature data [21]. S_1 RSD was low and constant, whereas S_2 RSD gradually decreased with lower temperatures, due to larger absolute anisotropy values obtained that reduced relative errors between measurements. This was confirmed by assessing the intensity ratio between the band of interest and the noise ($I_{HH\text{-}254}/I_{HH\text{-}noise}$), which increased with lower temperatures.

3.4 Anisotropies of xanthene dyes: To validate the dWGP accuracy at longer wavelengths, we used two anisotropy standards: Erythrosin B and Phloxine B [41]. Those fluorophores have similar absorbance and emission spectra (SI, Fig. S-5), and were interesting as they preserve high anisotropies under biologically relevant environmental conditions (*e.g.* HEPES buffer, pH 7.2 at 25°C) [42]. The solution anisotropies for Erythrosin B (6 μM), and Phloxine B (0.6 μM) measured using dWGP and TFP were almost identical (Figure 4) in the Rayleigh scatter free region (λ_{ex} = 500–530 nm). For Erythrosin, r = 0.243±0.002 (dWGP) versus 0.248±0.002 (TFP), and for Phloxine, r = 0.054±0.002 (dWGP) versus 0.060±0.002 (TFP). Despite a slight decrease due to the lower dWGP extinction coefficient in this spectral region, these values were almost in perfect agreement with Thompson *et al.*'s result [41], who obtained anisotropies of 0.243±0.002 and 0.055±0.002 using TFP and GTP.

3.5 Rayleigh scattering correction: ARMES generates a multidimensional data matrix ($\lambda_{ex} \times \lambda_{em} \times$ r) based on the anisotropy value at each point of the emission space (Figure 5). A threshold, set on the weakest intensity polarization measurement (HH for S_2 and VV for S_1), was necessary to remove low intensity regions which generate erroneous anisotropy values. Rayleigh scatter contamination is obvious in the anisotropy pattern, due to abnormally high values generated [2, 18]. It is possible to use a limited wavelength range to avoid scatter however, this was not acceptable for a multidimensional anisotropy standard. Furthermore, scattered light contamination also ruins the decomposition of EEM landscape [28, 29], thus for ARMES by EEM measurements, scatter correction is critical.

There are multiple methods available for dealing with Rayleigh scatter in EEM [15, 43-46]. The most widely used is classical interpolation, however it did not work well for perylene where emission and scatter overlap (SI, Fig. S-6). A more suitable method was to model the Rayleigh scatter as a separate set of components, to remove it from the original EEM [30]. This method transforms the Rayleigh scatter from a non-bilinear structure to a low rank bilinear structure, by shifting each contaminated emission spectrum, to form a line on the EEM landscape (bilinear element) rather than a diagonal (non-bilinear element, SI, Fig. S-7). Once all emission spectra were shifted, the signal was truncated to keep only the part related to the scatter, which can then be modelled by PCA or PARAFAC. The modelled scatter was then re-shifted back into the original matrix space, and subtracted from the raw signal.

To assess Rayleigh correction method efficiency, we measured the anisotropy dispersion within selected EEM regions. The rationale was that because anisotropy measurements are very sensitive to the presence of Raleigh scatter, a good correction method should generate EEM anisotropy dispersion values close to that obtained from the Rayleigh free TSFS data. Calculations were only implemented on the S_1 band with the most Rayleigh contamination. Two to four components were used to model the 1st order Rayleigh scatter as it was a low-rank bilinear element [30].

Modelling was more efficient for 1st order Rayleigh scatter correction than interpolation (Figure 6) as evidenced by the anisotropy dispersion being closer to TSFS values. PCA modelling was slightly better than PARAFAC which was possibly due to alignment imperfections during emission spectra shifting. This misalignment generated a small bi-linearity distortion adversely affecting PARAFAC. Three components were sufficient to model Rayleigh scatter, and this enabled the generation of anisotropy pattern (Figure 5 bottom) completely Rayleigh free (1st and 2nd order), with correct values retrieved in the scatter overlap regions. The perylene working range was thus increased, for S_1 from $\lambda_{ex/em}$ = 370-430/450-520 nm, to $\lambda_{ex/em}$ = 370-460/430-520, and for S_2 from $\lambda_{ex/em}$ = 240-270/430-490 nm to $\lambda_{ex/em}$ = 240-270/430-520 nm.

4. Conclusions

Replacing standard TFP polarizers with dWGP provided much superior UV transmittance and extinction ratios between 250 and 400 nm. dWGP performance was validated using perylene, Erythrosin B, and Phloxine B with the results were in excellent agreement with the literature [21, 41]. This confirmed anisotropy measurement accuracy using dWGP, over most of the important, short (λ_{ex} < 300 nm) and long (λ_{ex} > 300 nm) wavelength

regions required for protein analysis via intrinsic or extrinsic fluorescence. dWGP were easy to assemble using off-the-shelf components and fitted easily within the spectrometer sample chamber. The cost of this homebuilt dWGP was <4.5k€, 80% of which was filter costs.

Perylene in glycerol at temperatures between 25 and 10 °C was an ideal ARMES standard because it enabled the simultaneous collection of clearly discriminated positive and negative anisotropy values at different wavelengths. This characteristic was critical for a standard suitable for use with multidimensional measurements and chemometric data analysis. We also showed accurate Rayleigh scatter removal from EEM to provide correct anisotropy data using a chemometric approach. This modelling based correction also increased the working spectral range for perylene as a multidimensional anisotropy standard.

Implementing all these improvements, enabled accurate anisotropy and ARMES data to be collected via EEM measurements in the most important intrinsic fluorescence UV spectral region.

5. Supplemental information available

Supporting information is available with further details on the spectral and quantitative analyses.

Acknowledgements

Funding: The funders (Irish Research Council, IRC) had no role in study design, data collection and analysis, decision to publish, or preparation of the manuscript. The authors also acknowledge financial support from an IRC Postgraduate Scholarship (Grant #GOIPG/2015/3826). Agilent Technologies (Australia) are thanked for a fluorimeter loan.

Conflicting interests: The authors have declared that no conflicting interests exist.

References:

[1] Groza R C, Li B and Ryder A G 2015 Anisotropy resolved multidimensional emission spectroscopy (ARMES): A new tool for protein analysis *Anal. Chim. Acta* **886** 133-42

[2] Lakowicz J R 2006 *Principles of Fluorescence Spectroscopy* (New York: Springer)

[3] Bekard I B and Dunstan D E 2009 Tyrosine Autofluorescence as a Measure of Bovine Insulin Fibrillation *Biophys. J.* **97** 2521-31

[4] Togashi D M, Ryder A G and O'Shaughnessy D 2010 Monitoring local unfolding of bovine serum albumin during denaturation using steady-state and time-resolved fluorescence spectroscopy *J Fluoresc* **20** 441-52

[5] Lissi E, Calderon C and Campos A 2013 Evaluation of the Number of Binding Sites in Proteins from their Intrinsic Fluorescence: Limitations and Pitfalls *Photochem. Photobiol.* **89** 1413-6

[6] Sagoo K, Hirsch R, Johnston P, McLoskey D and Hungerford G 2014 Pre-denaturing transitions in human serum albumin probed time-resolved phosphorescence using *Spectrochimica Acta Part A-Molecular And Biomolecular Spectroscopy* **124** 611-7

[7] Warner I M, Christian G D, Davidson E R and Callis J B 1977 Analysis of Multicomponent Fluorescence Data *Anal. Chem.* **49** 564-73

[8] Patra D and Mishra A K 2002 Recent developments in multi-component synchronous fluorescence scan analysis *Trac-Trends in Analytical Chemistry* **21** 787-98

[9] Li B, Ryan P W, Shanahan M, Leister K J and Ryder A G 2011 Fluorescence EEM Spectroscopy for Rapid Identification and Quality Evaluation of Cell Culture Media Components. *Appl. Spectrosc.* **65** 1240-9

[10] Li B, Shanahan M, Calvet A, Leister K J and Ryder A G 2014 Comprehensive, quantitative bioprocess productivity monitoring using fluorescence EEM spectroscopy and chemometrics *Analyst* **139** 1661-71

[11] Jiang J H and Ozaki Y 2002 Self-modeling curve resolution (SMCR): Principles, techniques, and applications *Appl. Spectrosc. Rev.* **37** 321-45

[12] Antunes M C G and da Silva J 2005 Multivariate curve resolution analysis excitation-emission matrices of fluorescence of humic substances *Anal. Chim. Acta* **546** 52-9

[13] da Silva J C G E and Tauler R 2006 Multivariate curve resolution of synchronous fluorescence spectra matrices of fulvic acids obtained as a function of pH *Appl. Spectrosc.* **60** 1315-21

[14] de Juan A and Tauler R 2006 Multivariate curve resolution (MCR) from 2000: Progress in concepts and applications *Crit. Rev. Anal. Chem.* **36** 163-76

[15] Bro R 1997 PARAFAC. Tutorial and applications *Chemom. Intell. Lab. Syst.* **38** 149-71

[16] Andersen C and Bro R 2003 Practical aspects of PARAFAC modeling of fluorescence excitation-emission data *Journal of Chemometrics* **17** 200-15

[17] Chen H and Kenny J E 2012 Application of PARAFAC to a two-component system exhibiting Fluorescence Resonance Energy Transfer: from theoretical prediction to experimental validation *Analyst* **137** 153-62

[18] Groza R C, Calvet A and Ryder A G 2014 A fluorescence anisotropy method for measuring protein concentration in complex cell culture media *Anal. Chim. Acta* **821** 54-61

[19] Groza R C 2016 Anisotropy Resolved Multi-dimensional Emission Spectroscopy (ARMES): A new tool for the quantitative and structural analysis of proteins. In: *Chemistry,* (Galway, Ireland: National University of Ireland Galway)

[20] Lakowicz J R 2006 *Principles of Fluorescence Spectroscopy, 3rd Edition,* ed Springer

[21] Barkley M D, Kowalczyk A A and Brand L 1981 Fluorescence decay studies of anisotropic rotations of small molecules *The Journal of chemical physics* **75** 3581-93

[22] Balter A and Szubiakowski J 1993 Fluorescence probes of viscosity: a comparative study of the fluorescence anisotropy decay of perylene and 3,9-Dibromoperylene in glycerol *Journal of Fluorescence* **3** 247-9

[23] Szubiakowski J, Balter A, Nowak W, Kowalczyk A, Wisniewski K and Wierzbowska M 1996 Anisotropic reorientation of perylene and 3,9-dibromoperylene in glycerol: fluorescence anisotropy decay and quantum-mechanical study *Chemical Physics* **208** 283-96

[24] Johansson J B-A 1990 Limiting Fluorescence Anisotropies of Perylene and Xanthene Derivatives *Journal of the Chemical Society, Faraday Transactions* **86** 2103-7

[25] Prazeres T J V, Fedorov A, Barbosa S P, Martinho J M G and Berberan-Santos M N 2008 Accurate determination of the limiting anisotropy of rhodamine 101. Implications for its use as a fluorescence polarization standard *J. Phys. Chem. A* **112** 5034-9

[26] Pantke E R and Labhart H 1973 Influence of excess excitation energy on rotational relaxation of molecules in solution *Chemical Physics Letters* **23** 476-81

[27] Tauler R, Marques I and Casassas E 1998 Multivariate curve resolution applied to three-way trilinear data: Study of a spectrofluorimetric acid–base titration of salicylic acid at three excitation wavelengths *Journal of Chemometrics* **12** 55-75

[28] Rinnan A and Andersen C M 2005 Handling of first-order Rayleigh scatter in PARAFAC modelling of fluorescence excitation-emission data *Chemom. Intell. Lab. Syst.* **76** 91-9

[29] Murphy K R, Stedmon C A, Graeber D and Bro R 2013 Fluorescence spectroscopy and multi-way techniques. PARAFAC *Analytical Methods* **5** 6557-66

[30] Rinnan Å, Booksh K S and Bro R 2005 First order Rayleigh scatter as a separate component in the decomposition of fluorescence landscapes *Analytica Chimica Acta* **537** 349-58

[31] Weber T, Fuchs H-J, Schmidt H, Kley E-B and Tunnermann A 2009 Wire-grid polarizer for the UV spectral region *Proceedings of SPIE* **7205**

[32] Pang Y T, Meng G W, Zhang Y, Fang Q and Zhang L D 2003 Copper nanowire arrays for infrared polarizer *Applied Physics A* **76** 533-6

[33] Lawaetz A J and Stedmon C A 2009 Fluorescence Intensity Calibration Using the Raman Scatter Peak of Water *Appl. Spectrosc.* **63** 936-40

[34] Zhang J Z and Grant C D 2008 *Annual Review of Nano Research,* ed G Cao and C J Brinker: World Scientific)

[35] Destrampe K A and Hieftje G M 1993 New Instrumentation for Use in Excitation-Emission Fluorescence-Polarization Measurements *Applied Spectroscopy* **47** 1548-54

[36] Mann T L and Krull U J 2003 Fluorescence polarization spectroscopy in protein analysis *The Analyst* **128** 313-7

[37] Zaman G J, Garritsen A, De Boer T and Van Boeckel C A 2003 Fluorescence assays for high-throughput screening of protein kinases *Combinatorial Chemistry & High Throughput Screening* **6** 313-20

[38] Lea W A and A. S 2011 Fluorescence polarization assays in small molecule screening *Expert Opinion on Drug Discovery* **6** 17-32

[39] Zondervan R, Kulzer F, Berkhout G C G and Orrit M 2007 Local viscosity of supercooled glycerol near Tg probed by rotational diffusion of ensembles and single dye molecules *PNAS* **104** 12628-33

[40] Schroter K and Donth E 2000 Viscosity and shear response of the dynamic glass transition of glycerol *Journal of Chemical Physics* **113** 9101-8

[41] Thompson R B, Gryczynski I and Malicka J 2002 Fluorescence Polarization Standards for High-Throughput Screening and Imaging *Biotechniques* **32** 34-42

[42] Duarte P, Ferreira D P, Ferreira Machado I, Vieira Ferreira L F, Rodriguez H B and Sam Roman E 2012 Phloxine B as a probe for entrapment in microcrystalline cellulose *Molecules* **17** 1602-16

[43] JiJi R D and Booksh K S 2000 Mitigation of Rayleigh and Raman spectral interferences in multiway calibration of excitation-emission matrix fluorescence spectra *Anal. Chem.* **72** 718-25

[44] Wentzell P D, Nair S S and Guy R D 2001 Three-way analysis of fluorescence spectra of polycyclic aromatic hydrocarbons with quenching by nitromethane *Analytical Chemistry* **73** 1408-15

[45] Thygesen L G, Rinnan A, Barsberg S and Moller J K S 2004 Stabilizing the PARAFAC decomposition of fluorescence spectra by insertion of zeros outside the data area *Chemom. Intell. Lab. Syst.* **71** 97-106

[46] Bahram M, Bro R, Stedmon C and Afkhami A 2006 Handling of Rayleigh and Raman scatter for PARAFAC modeling of fluorescence data using interpolation *J. Chemom.* **20** 99-105

Tables.

Polarizers	Average r value for λex/em = 240-270/430-490 nm (S_2)	STD	Average r value for λex/em = 370-430/450-520 nm (S_1)	STD
WGP	–0.024	± 0.003	0.180	± 0.004
dWGP	–0.034	± 0.004	0.202	± 0.001
TFP[1]	Not measurable	N/A	0.216	± 0.001

Table 1: Anisotropy and Standard deviations (STD) values for a 1μM perylene in glycerol solution obtained in the short and long wavelength regions with the different filter combinations. Data measured in triplicate.

	r ± STD (RSD) λex/em = 240-270/430-490 nm	Barkley λ_{ex} = 256 nm	$\frac{I_{HH-254}}{I_{HH-noise}}$	r ± STD (RSD) λex/em = 370-430/450-520 nm	Barkley λ_{ex} = 430 nm	$\frac{I_{VV-414}}{I_{VV-noise}}$
25°C	–0.034 ± 0.004 (11.76%)	–0.031 ± 0.002	18.9	0.202 ± 0.001 (0.50%)	0.197 ± 0.002	37.6
20°C	–0.052 ± 0.003 (5.77%)	–0.052 ± 0.002	19.2	0.229 ± 0.003 (1.31%)	0.231 ± 0.002	38.1
15°C	–0.071 ± 0.003 (4.23%)	–0.076 ± 0.002	19.5	0.256 ± 0.002 (0.78%)	0.260 ± 0.002	38.6
10°C	–0.092 ± 0.003 (3.26%)	–0.097 ± 0.002	20.0	0.280 ± 0.001 (0.36%)	0.285 ± 0.002	39.1

Table 2: Average of anisotropy values obtained for 1μM solution of perylene in glycerol using dWGP at different temperatures, in the low (λ_{ex} = 244-264 nm) and high (λ_{ex} = 390-430 nm) wavelength region; Intensity ratios of I_{HH} (λ_{ex} = 254 nm) to $I_{HH\text{-}noise}$ (average λ_{ex} = 280-300 nm), and I_{VV} (λ_{ex} = 414 nm) to $I_{VV\text{-}noise}$ (average λ_{ex} = 280-300 nm). Data were collected in triplicate and 21/41 points were used respectively to obtain those results (2 nm data interval).

[1] TFP could not measure anisotropy for the S_2 band.

Figure Captions:

Figure 1: Transmission spectra of TFP and WGP filter combinations, collected separately first (A, C) as well as in pairs (B, D). The transmittance spectra of the pair of dWGP (total of 4 filters) is also presented (E) and compared with transmittance spectra of a single WGP, in the region of interest (F). Both horizontal (H) and vertical (V) positions were measured. The center of the polarizer was aligned normal to the light beam.

Figure 2: HH spectra of 1 μM perylene solution in glycerol obtained at 25°C using (left) TFP and (right) dWGP.

Figure 3: Overlay of polarized excitation (A / λ_{em} = 444 nm) and emission spectra (B / λ_{ex} = 254 nm, C / λ_{ex} = 440 nm) collected using WGP, dWGP, and TFP, with calculated anisotropies. The spectra and anisotropy represent the average values obtained for 3 replicate measurements of a 1μM solution of perylene in 100% glycerol. For clarity, only VV spectra are shown for TFP and dWGP

Figure 4: Overlay of polarized excitation (A / λ_{em} = 548 nm, C / λ_{em} = 554 nm) and emission spectra (B / λ_{ex} = 520 nm, D / λ_{ex} = 520 nm) collected using dWGP and TFP for Erythrosin B and Phloxine B, with calculated anisotropies. The spectra and anisotropy are average values obtained from 3 measurements. For clarity, only VV spectra are shown for TFP.

Figure 5: Anisotropy-EEM contour plots of 1μM perylene in 100% glycerol collected with **a** 10% threshold of the HH scan for λ_{ex} = 230-340 nm, and VV scan for λ_{ex} = 342-470 nm. Data collected using dWGP, in triplicate at 25°C. (Top) The uncorrected anisotropy pattern, and (Bottom) Final corrected anisotropy pattern after Rayleigh correction using the modelling method. The boxes show the increase in the working range obtained by correction.

Figure 6: Efficiency comparison between modelling (PCA, PARAFAC) and interpolation methods for correcting 1st order Rayleigh scatter by calculating r dispersion versus threshold. TSFS data were used as a reference. Calculations were done using only the S_1 band from a 1 μM perylene glycerol solution (collected on dWGP, in triplicate, 25°C).

Figures:

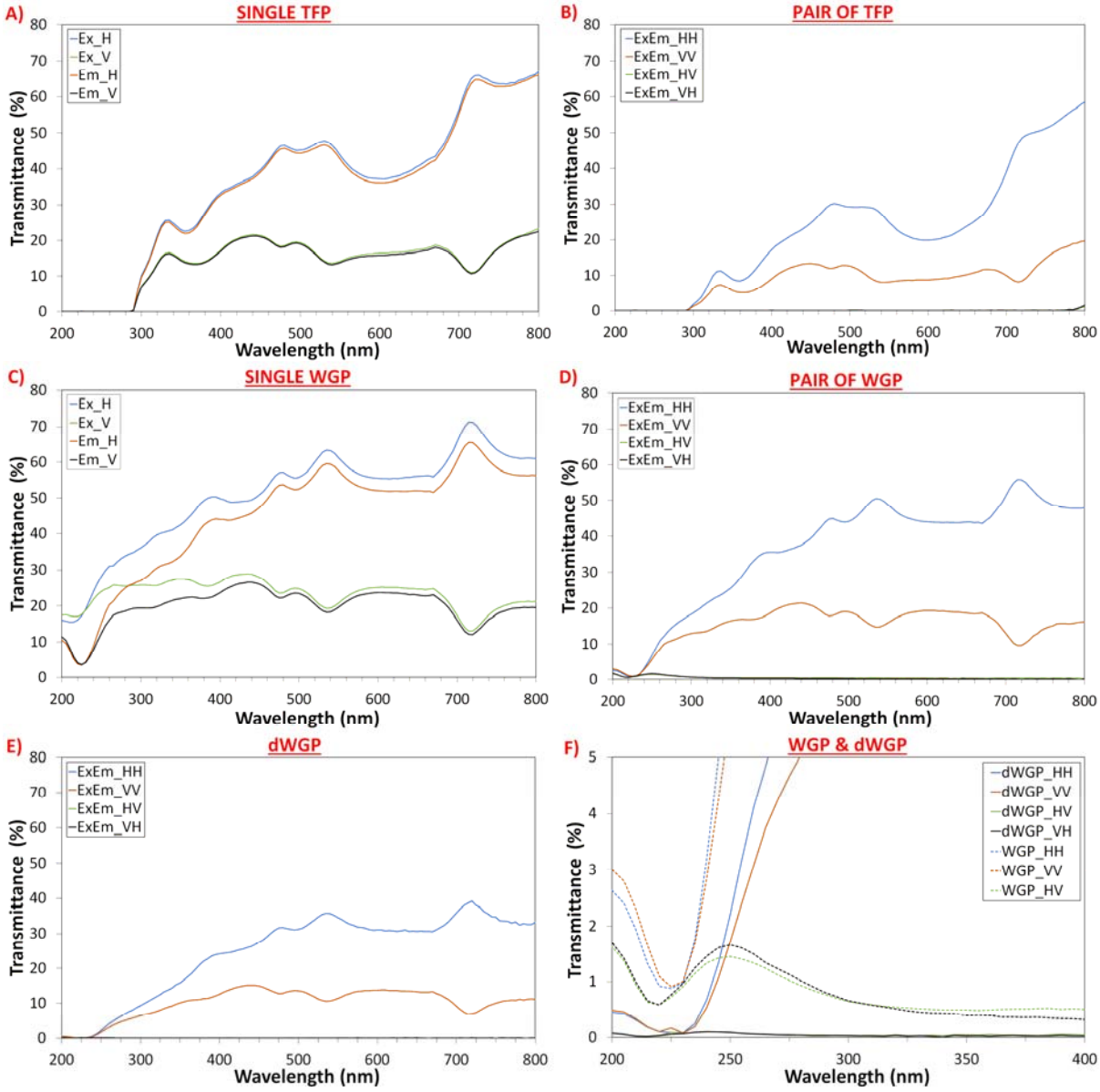

Figure 1

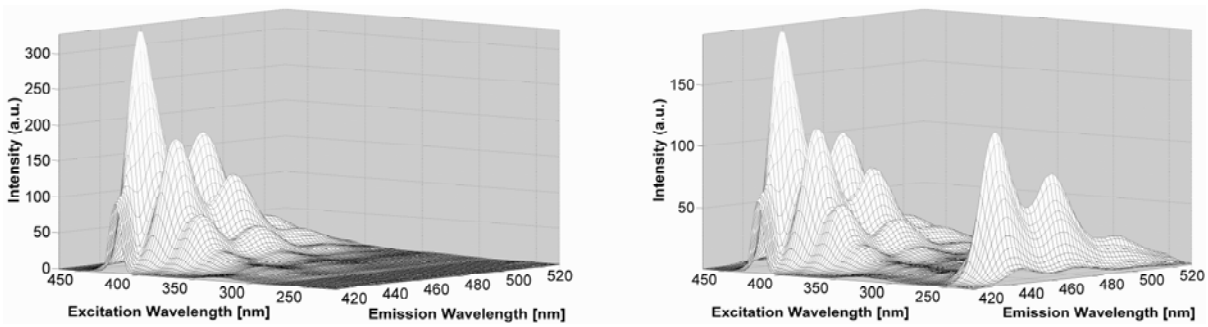

Figure 2

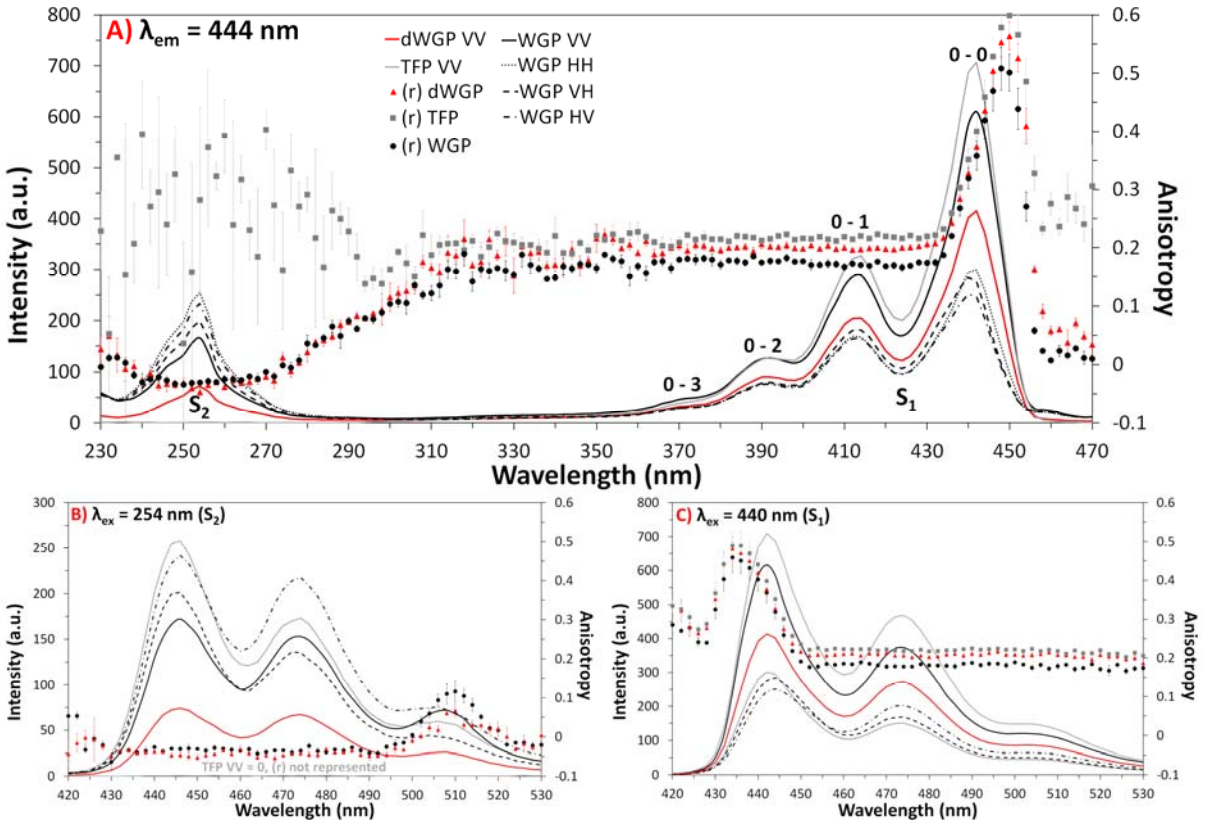

Figure 3

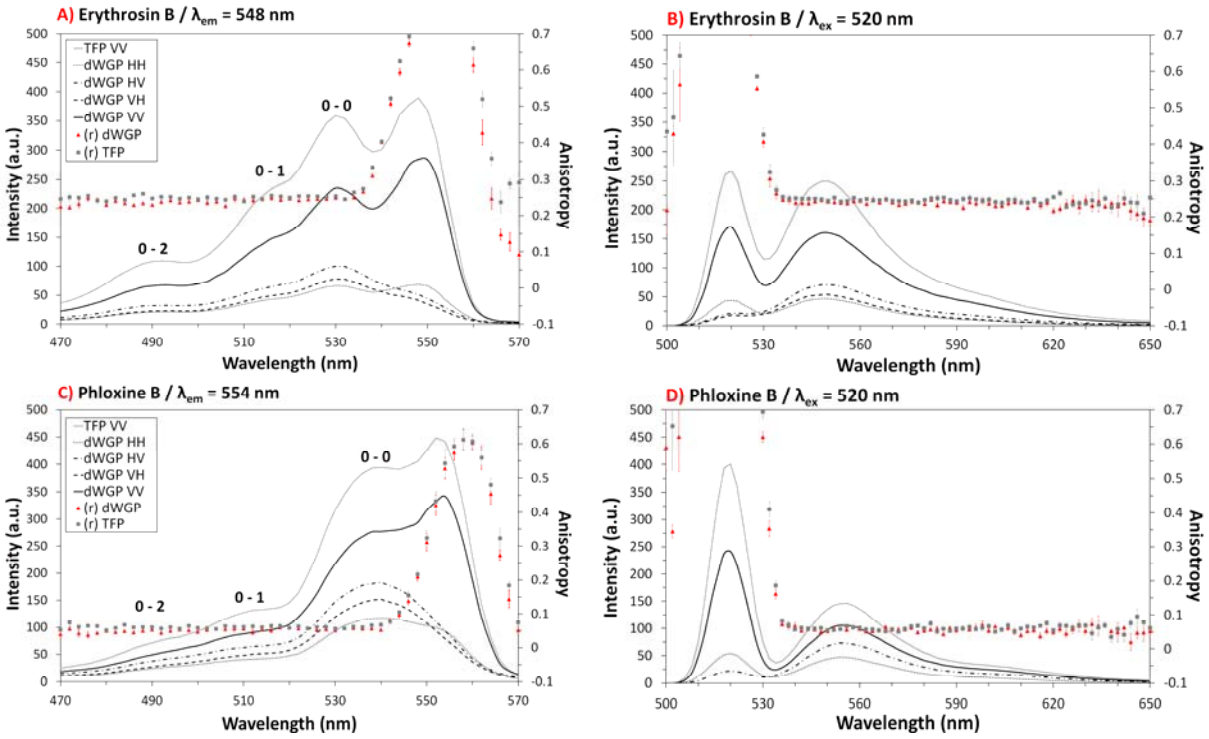

Figure 4

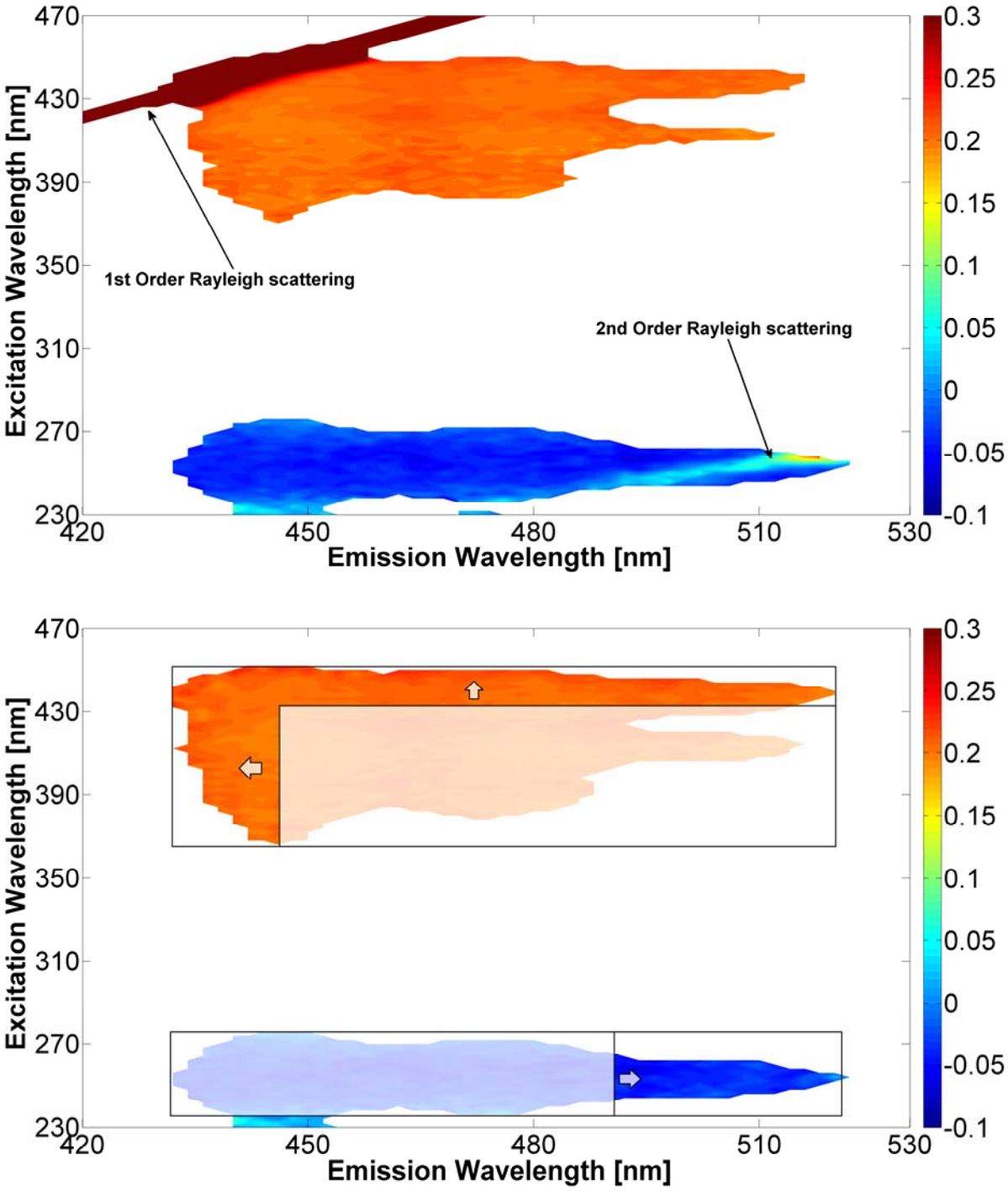
Excitation Wavelength [nm]
Emission Wavelength [nm]
1st Order Rayleigh scattering
2nd Order Rayleigh scattering
470
430
390
350
310
270
230
420
450
480
510
530
0.3
0.25
0.2
0.15
0.1
0.05
0
-0.05
-0.1

Figure 5

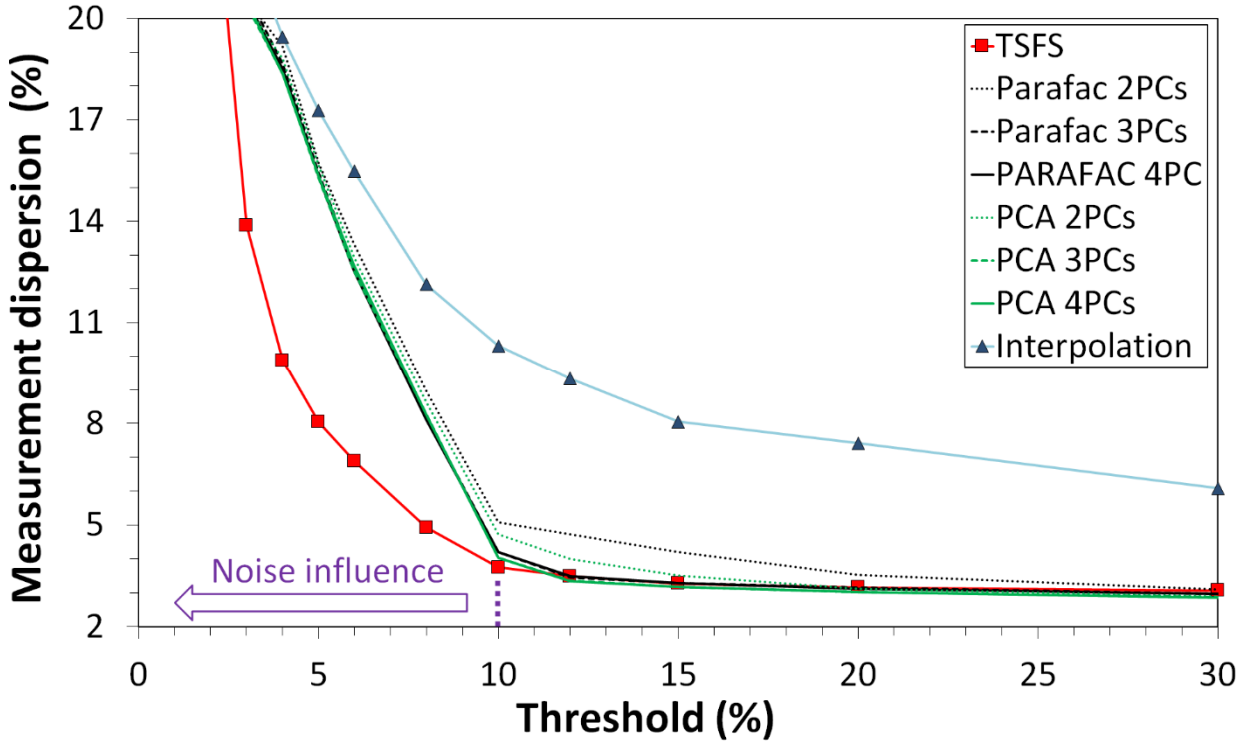
Measurement dispersion (%)
20
17
14
11
8
5
2
0
5
10
15
20
25
30
Threshold (%)
TSFS
Parafac 2PCs
Parafac 3PCs
PARAFAC 4PC
PCA 2PCs
PCA 3PCs
PCA 4PCs
Interpolation
Noise influence

Figure 6